Controlled-NOT logic with nonresonant Josephson phase qubits

Andrei Galiautdinov*
Department of Physics and Astronomy, University of Georgia, Athens, Georgia 30602, USA
(Dated: December 30, 2008)

We establish theoretical bounds on qubit detuning for high fidelity controlled-NOT logic gate implementations with weakly coupled Josephson phase qubits. It is found that the value of qubit detuning during the entangling pulses must not exceed $2g$ for two-step, and g for single-step control sequences, where g is the relevant coupling constant.

PACS numbers: 03.67.Lx, 03.65.Fd, 85.25.-j

I. INTRODUCTION

In our previous work on steering with Josephson phase qubits [1] we found two peculiar single-step controlled-NOT (CNOT) implementations involving off-resonance qubits detuned by the amount smaller than the characteristic coupling constant. Does the detuning always have to be so small? What happens if it gets larger?

These questions seem to be important on several counts.

Firstly, the majority of entangling gate designs proposed in the literature assume resonant qubits [2, 3, 4, 5, 6, 7, 8, 9]. (However, see Refs. [10, 11] for notable exceptions.) This is hardly surprising since in the rotating wave approximation (RWA) typically used to analyze superconducting qubits the resonant condition leads to relatively simple and easily solvable Hamiltonians containing no local σ_k^z terms. This works well when the system consists of only two qubits. However, it is reasonable to expect that when thousands of such qubits are assembled into an integrated circuit, maintaining them on resonance will become a difficult task. How then can we be sure that an architecture involving detuned qubits is able to reliably generate universal gates, such as, for example, a CNOT gate?

Secondly, some qubits may be fabricated with various defects preventing them from being tuned to resonance exactly. Would they still be usable? And what if for some applications it becomes advantageous (or even necessary) to use qubits with intrinsically different level splittings?

Thirdly, we should also keep in mind that detuning is routinely used in actual experiments to "decouple" the qubits in order to perform local (that is, nonentangling) operations [2, 12, 13, 14]. It would be useful if, after such decoupling is performed, we do not have to worry about bringing the qubits back to exact resonance when doing subsequent entangling operations.

Additionally, from the purely theoretical viewpoint, decoupling provides a useful limit against which to check our calculations. If at larger detuning the interaction is expected to lose its entangling properties, we must be able to predict a crossover into the regime when the gate fidelity (of the CNOT, in our case) starts to deteriorate. Thus, the primary goal of this paper will be to establish the exact conditions under which such crossover occurs for previously proposed CNOT implementations involving superconducting qubits.

The paper is organized as follows:

In Section III we introduce the Hamiltonian for capacitively and inductively coupled Josephson phase qubits. Since there is an infinite number of possible local drives and rotating frames to choose from, it will be necessary to limit our discussion to situations that are simple and yet powerful enough to provide some new and interesting physical insights. Our specific choices for Rabi pulses and rotating frames will be made in Eqs. (3), (4), and (6) of that Section.

In Section IV we generalize to finite detuning the familiar two-step CNOT sequence involving a local π-pulse sandwiched between two entanling operations. The exact bound on detuning that guarantees generation of the perfect (in the RWA) controlled-NOT logic gate will then be given in Eq. (21).

In Section V we numerically solve the single-step case. We will see that in that case the restriction on detuning for perfect CNOT generation is somewhat stronger than in the two-step case (Eq. (27)).

In Section VI we present optimal results for approximate CNOT gates at detuning larger than maximally allowed. We will see how the Makhlin invariants and fidelity of the optimized gates deviate from their ideal CNOT values. We will also simulate the Weyl chamber steering trajectories corresponding to such optimized gates.

We conclude in Section VII with a brief summary of our results.

*Electronic address: ag@physast.uga.edu

II. NOTATION

In what follows, we will use the notation that is convenient for Lie algebraic manipulations,

$$\begin{aligned} &X_k = \frac{i}{2}\sigma_k^x,\ Y_k = \frac{i}{2}\sigma_k^y,\ Z_k = \frac{i}{2}\sigma_k^z, \quad (k=1,2),\\ &XX = \frac{i}{2}\sigma_2^x\sigma_1^x,\ YY = \frac{i}{2}\sigma_2^y\sigma_1^y,\ ZZ = \frac{i}{2}\sigma_2^z\sigma_1^z,\\ &XY = \frac{i}{2}\sigma_2^x\sigma_1^y,\ YX = \frac{i}{2}\sigma_2^y\sigma_1^x. \end{aligned} \tag{1}$$

Notice, that $[XX, YY] = [XY, YX] = 0$, and ZZ commutes with each of the XX, YY, XY, YX operators.

Why is this notation convenient?

Consider the following transformation (called "going to a rotated frame") on the Lie algebra $su(4)$ of the two-qubit system:

$$XX \longrightarrow e^{-\theta Z_1} XX e^{\theta Z_1} = XX\cos\theta + XY\sin\theta. \tag{2}$$

This transformation can be nicely interpreted as a rotation of vector XX by an angle θ in the *real* vector space spanned by the generators of the group SU(4). This is how the continuous group acts on its Lie algebra. Mathematicians call it the adjoint representation. The algebra plays the role of the representation space for its own group.

Since we do work at the level of algebra, and not at the level of the Hilbert space when discussing equivalence classes of gates, this is a very convenient notation. It simplifies things. Also notice how naturally the periodicity of 2π appears at this level of description.

Now, if we were to write the same transformation in terms of the Pauli matrices, we would have to remember to put in the imaginary unit i and the factors of $1/2$ in the exponents on the left hand side of Eq. (2),

$$e^{-i\theta\sigma_z^1/2}(\sigma_2^x\sigma_1^x)e^{i\theta\sigma_z^1/2} = (\sigma_2^x\sigma_1^x)\cos\theta + (\sigma_2^x\sigma_1^y)\sin\theta,$$

breaking its beautiful symmetry.

III. THE HAMILTONIAN

When restricted to the computational subspace, the Hamiltonian for two coupled Josephson phase qubits, one of which is driven by a resonant rf pulse, is given by

$$\begin{aligned} iH(t) &= -\omega Z_1 - (\omega+\delta)Z_2 \\ &\quad +2\Omega_1\cos(\omega t)\,X_1 + 2(gYY + \tilde{g}ZZ), \end{aligned} \tag{3}$$

where $g, \tilde{g} \ll \omega$ are the coupling constants, ω is the level splitting of the first qubit, $|\delta| \ll \omega$ is the detuning, and Ω_1 is the corresponding Rabi frequency. Here we assume that $g \simeq \Omega_1$, which differs from the condition $g \ll \Omega_1 \ll \omega$ adopted in Ref. [10]. For realistic systems, $\omega \approx 10$ GHz, $g \approx 10$ MHz. For capacitive coupling, $\tilde{g} = 0$; for inductive coupling, $\tilde{g} \lesssim 0.1g$.

In the doubly rotating frame defined by $e^{iH_0t}(\dots)e^{-iH_0t}$, with $iH_0 \equiv -\omega(Z_1 + Z_2)$, after averaging over fast oscillations, the system Hamiltonian is time-independent,

$$iH_{\rm RWA} = -\delta Z_2 + \Omega_1 X_1 + i\mathcal{H} + \tilde{g}ZZ, \tag{4}$$

with

$$i\mathcal{H} = g(XX + YY) = ig\begin{pmatrix} 0&0&0&0\\ 0&0&1&0\\ 0&1&0&0\\ 0&0&0&0 \end{pmatrix}. \tag{5}$$

Alternatively, to perform a useful consistency check, we consider another rotating frame defined by $e^{i\hat{H}_0t}(\dots)e^{-i\hat{H}_0t}$, with $i\hat{H}_0 = -\omega Z_1 - (\omega+\delta)Z_2$. In this frame, the RWA Hamiltonian is

$$i\hat{H}_{\rm RWA}(t) = \Omega_1 X_1 + i\hat{\mathcal{H}}(t) + \tilde{g}ZZ, \tag{6}$$

where now we have a slowly varying interaction term given by

$$\begin{aligned} i\hat{\mathcal{H}}(t) &= g\left[(XX+YY)\cos(\delta t) + (YX-XY)\sin(\delta t)\right] \\ &= ig\begin{pmatrix} 0&0&0&0\\ 0&0&e^{-i\delta t}&0\\ 0&e^{+i\delta t}&0&0\\ 0&0&0&0 \end{pmatrix}. \end{aligned} \tag{7}$$

The central block of this matrix has the form of a rotating drive for a spin-1/2 system for which the analytical solution is well known [19]. This observation will prove helpful for calculations in Section IV.

We will now show how these two RWA Hamiltonians lead to locally equivalent CNOT implementations.

IV. TWO-STEP CNOT

The well-known two-step CNOT implementation for *resonant* ($\delta = 0$) qubits has control sequence [15, 16]

$$\mathrm{CNOT}_{(2)} = e^{i(\pi/4)}R_{\rm post}\left[U(t_{(2)})e^{-\pi X_1}U(t_{(2)})\right]R_{\rm pre}, \tag{8}$$

with $t_{(2)} = \pi/4g$, where

$$\begin{aligned} U(t_{(2)}) &= e^{-t_{(2)}(g(XX+YY)+\tilde{g}ZZ)} \\ &= e^{-(\pi\tilde{g}/4g)ZZ}\begin{pmatrix} 1&0&0&0\\ 0&1/\sqrt{2}&-i/\sqrt{2}&0\\ 0&-i/\sqrt{2}&1/\sqrt{2}&0\\ 0&0&0&1 \end{pmatrix}, \end{aligned} \tag{9}$$

and $R_{\rm post,pre}$ are some local rotations. We will choose

$$R_{\rm post} = e^{-(\pi/2)Y_2},\ R_{\rm pre} = e^{-(\pi/2)Z_2}e^{+(\pi/2)(X_2+X_1)}. \tag{10}$$

Of particular importance to us is the entangling part $U(t)e^{-\pi X_1}U(t)$ that determines the local equivalence

class of the full gate. In our case the local class is controlled-NOT whose canonical representative in the computational basis is defined to be

$$\mathrm{CNOT} \equiv \begin{pmatrix} 1 & 0 & 0 & 0 \\ 0 & 1 & 0 & 0 \\ 0 & 0 & 0 & 1 \\ 0 & 0 & 1 & 0 \end{pmatrix} \in \mathrm{U}(4),\ \det(\mathrm{CNOT}) = -1. \tag{11}$$

We ask the following question: If $|\delta| > 0$ (*detuned* qubits), can we still use the sequence in Eq. (8) to generate a CNOT gate, possibly with *different* gate time and different pre- and post-rotations? The answer to this question turns out to be "Yes", provided δ is restricted in a certain way.

Setting $\Omega_1 = 0$ in Eqs. (4) and (6) gives the time evolution operator

$$U(t) = e^{-t\tilde{g}ZZ} \begin{pmatrix} e^{i\delta t/2} & 0 & 0 & 0 \\ 0 & u & -iv & 0 \\ 0 & -iv & u^* & 0 \\ 0 & 0 & 0 & e^{-i\delta t/2} \end{pmatrix} \tag{12}$$

in frame 1, and

$$\hat{U}(t) = e^{-t\tilde{g}ZZ} \begin{pmatrix} 1 & 0 & 0 & 0 \\ 0 & ue^{-i\delta t/2} & -ive^{-i\delta t/2} & 0 \\ 0 & -ive^{i\delta t/2} & u^* e^{i\delta t/2} & 0 \\ 0 & 0 & 0 & 1 \end{pmatrix} \tag{13}$$

in frame 2, where

$$u = \cos\left(\frac{\sqrt{\delta^2+4g^2}}{2}t\right) + \frac{i\delta}{\sqrt{\delta^2+4g^2}}\sin\left(\frac{\sqrt{\delta^2+4g^2}}{2}t\right), \tag{14}$$

$$v = \frac{2g}{\sqrt{\delta^2+4g^2}}\sin\left(\frac{\sqrt{\delta^2+4g^2}}{2}t\right). \tag{15}$$

In both frames the Makhlin invariants [17] of $U(t)e^{-\pi X_1}U(t)$ are

$$G_1 = \left(\frac{\delta^2 + 8g^2\cos^2\left(\frac{\sqrt{\delta^2+4g^2}}{2}t\right) - 4g^2}{\delta^2+4g^2}\right)^2, \tag{16}$$

and

$$\begin{aligned} G_2 = {} & (3\delta^4 + 8\delta^2 g^2\left[1 + 2\cos(t\sqrt{\delta^2+4g^2})\right] \\ & + 16g^4\left[2 + \cos(2t\sqrt{\delta^2+4g^2})\right])/\left(\delta^2+4g^2\right)^2, \end{aligned} \tag{17}$$

and are independent of the ZZ coupling. This shows that for any t the resulting gates are represented by the same point on the (XX, YY)-plane of the Weyl chamber (see [1, 16] for discussion). Since CNOT class corresponds to $G_1 = 0$, $G_2 = 1$, we get

$$t_{(2)} = \frac{\pi - \arccos\left(\delta^2/4g^2\right)}{\sqrt{\delta^2+4g^2}}, \tag{18}$$

with the limit $t_{(2)} \to \pi/4g$ trivially recovered for vanishing detuning.

For example, for $\tilde{g} = 0$, $\delta = 1.00g$, we get $t_{(2)} = 1.0383\pi/4g$. The corresponding CNOT gate is given by Eq. (8), where now

$$\begin{aligned} U(t_{(2)}) &= \begin{pmatrix} 0.9180+0.3965i & 0 & 0 & 0 \\ 0 & 0.6124+0.3536i & -0.7071i & 0 \\ 0 & -0.7071i & 0.6124-0.3536i & 0 \\ 0 & 0 & 0 & 0.9180-0.3965i \end{pmatrix}, \\ R_{\mathrm{post}} &= e^{-(\pi/2)Y_2}e^{-(\pi/2)(\alpha_2 Z_2 + \alpha_1 Z_1)}, \quad R_{\mathrm{pre}} = e^{-(\pi/2)((1+\alpha_2)Z_2 + \alpha_1 Z_1)}e^{+(\pi/2)(X_2+X_1)}, \end{aligned} \tag{19}$$

with $\alpha_2 = 0.5929$, $\alpha_1 = 0.2596$ in frame 1, and

$$\begin{aligned} \hat{U}(t_{(2)}) &= \begin{pmatrix} 1 & 0 & 0 & 0 \\ 0 & 0.7024+0.0817i & -0.2804-0.6491i & 0 \\ 0 & 0.2804-0.6491i & 0.7024-0.0817i & 0 \\ 0 & 0 & 0 & 1 \end{pmatrix}, \\ R_{\mathrm{post}} &= e^{-(\pi/2)Y_2}e^{-(\pi/2)\tilde{\beta}Z_2}, \\ R_{\mathrm{pre}} &= e^{-(\pi/2)(1+\beta)Z_2}e^{+(\pi/2)(X_2+X_1)}, \end{aligned} \tag{20}$$

with $\tilde{\beta} = -0.1858$, $\beta = 0.3333$ in frame 2. Here, the pre- and post-rotations (cf. Eq. (10)) needed to generate the perfect in the rotating wave approximation canonical controlled-NOT gate have been found numerically. Notice that the two-step control sequence works only for

$$|\delta| \leq 2g \ll \omega. \tag{21}$$

V. SINGLE-STEP CNOT

Here, for simplicity, we limit our discussion to the RWA Hamiltonian given in Eq. (4) with $\tilde{g} = 0$ (capacitive

coupling). [In this case, a single Rabi term suffices to implement a CNOT gate. When $\tilde{g} \neq 0$, an additional local Rabi drive $\sim \Omega_2 X_2$ must be applied to the second qubit.] The CNOT sequence [1, 18] is then

$$\mathrm{CNOT}_{(1)} = e^{i(5\pi/4)} R_{\mathrm{post}} U(t_{(1)}) R_{\mathrm{pre}}, \tag{22}$$

where $t_{(1)} = \pi/2g$, $\Omega_1 = g\sqrt{(4n)^2 - 1}$, $n = 1, 2, 3, \ldots$,

$$\begin{aligned} U(t_{(1)}) &= e^{-t_{(1)}[\Omega_1 X_1 + g(XX+YY)]} \\ &= \frac{(-1)^n}{\sqrt{2}} \begin{pmatrix} 1 & 0 & 0 & -i \\ 0 & 1 & -i & 0 \\ 0 & -i & 1 & 0 \\ -i & 0 & 0 & 1 \end{pmatrix}, \end{aligned} \tag{23}$$

and

$$R_{\mathrm{post}} = e^{-(\pi/2)Y_2}, \; R_{\mathrm{pre}} = e^{-(\pi/2)Z_2} e^{+(\pi/2)(X_2 - X_1)}. \tag{24}$$

In order to generalize this single-step implementation to finite detuning, we optimize the gate parameters $t_{(1)}$ and Ω_1 of

$$U(t_{(1)}) = e^{-t_{(1)}[-\delta Z_2 + \Omega_1 X_1 + g(XX+YY)]} \tag{25}$$

using Nelder-Mead simplex direct search with bound constraints for the minimum of the distance from the CNOT class defined by

$$\begin{aligned} d^2(\Omega_1, t_{(1)}) \; := \; & |G_1(\Omega_1, t_{(1)}) - G_1(\mathrm{CNOT})|^2 \\ & + |G_2(\Omega_1, t_{(1)}) - G_2(\mathrm{CNOT})|^2, \end{aligned} \tag{26}$$

with $G_{1,2}(\Omega_1, t_{(1)})$ being the Makhlin invariants of $U(t_{(1)})$. It is important to keep in mind that the distance function introduced in Eq. (26) is *not* a measure of the gate fidelity. Infinitely many gates — all differing from each other by arbitrary local rotations — may have the same value of $d^2(\Omega_1, t_{(1)})$. Once the entangling part $U(t_{(1)})$ is found to have $d^2(\Omega_1, t_{(1)}) = 0$, it can then be made into the canonical CNOT gate by additional local rotations.

Actual experiments motivate this choice of the distance function. It is generally believed that doing local rotations is easy, but performing entanglement is difficult. Thus, if by using experimentally available interaction and the local controls we can somehow steer the system into the "right" equivalence class, then making the actual target gate will be relatively straightforward.

Performing the optimization we find that in order to generate the exact CNOT in the single-step case the detuning must be restricted by

$$|\delta| \leq g \ll \omega. \tag{27}$$

For example, for maximally allowed $\delta = g$, we get $t_{(1)} = 1.2753\pi/2g$, $\Omega_1 = 3.7781g$. The resulting gate is given by Eq. (22) with

$$\begin{aligned} U(t_{(1)}) &= \begin{pmatrix} -0.2553 - 0.4300i & 0.4821 - 0.1324i & -0.4821 + 0.1324i & 0.5001i \\ 0.4821 - 0.1324i & -0.0001 + 0.5001i & 0.5001i & 0.4821 + 0.1324i \\ -0.4821 + 0.1324i & 0.5001i & -0.0001 - 0.5001i & 0.4821 + 0.1324i \\ 0.5001i & 0.4821 + 0.1324i & 0.4821 + 0.1324i & -0.2553 + 0.4300i \end{pmatrix}, \\ R_{\mathrm{post}} &= e^{-(\pi/2)Y_2} e^{-(\pi/2)(\alpha_2 Z_2 + \alpha_1 Z_1)}, \quad R_{\mathrm{pre}} = e^{-(\pi/2)((1+\alpha_2)Z_2 + \alpha_1 Z_1)} e^{+(\pi/2)(X_2 - (1+\gamma_1)X_1)}, \end{aligned} \tag{28}$$

where $\alpha_2 = 0.8294$, $\alpha_1 = -0.1705$, $\gamma_1 = -0.9998$.

To visualize how this gate is reached in the course of the unitary evolution we simulate the Weyl chamber steering trajectory $\vec{c}(t) = (c_1(t), c_2(t), c_3(t))$ for the above mentioned values of the gate parameters. The goal here is to establish a correspondence [16],

$$U(t) \sim e^{-c_1(t)XX - c_2(t)YY - c_3(t)ZZ}, \tag{29}$$

between the physical gate $U(t)$ and the unphysical matrix exponential that formally resides in the same local equivalence class as $U(t)$. The time-dependent vector $\vec{c}(t)$ then represents the dynamically generated class at every moment of system's evolution. Figures 1 and 2 show how the CNOT class that has $\vec{c} = (\pi/2, 0, 0)$ is generated in our single-step example with $\delta = g$.

For other values of qubit detuning, the gate parameters required to implement perfect two-step and single-step CNOT logic are listed in Table I.

VI. WHAT HAPPENS AT LARGER DETUNING?

When detuning exceeds the limits set in Eqs. (21) and (27), our implementations begin to deviate from their perfect controlled-NOT form. To visualize how that happens, we again search for the gate parameters that produce the gates that belong to the local equivalence classes closest to CNOT in the sense of the distance function defined in Eq. (26). The corresponding results for single-

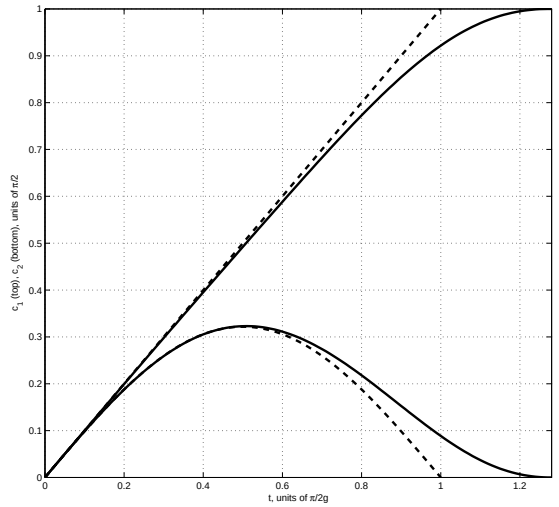

FIG. 1: Time dependence of c_1 (top curve) and c_2 (bottom curve) for single-step CNOT implementation with capacitively coupled Josephson phase qubits at maximal detuning, $\delta = g$. Here, $c_3 = 0$ at all times. Dashed curves represent the resonant case, $\delta = 0$.

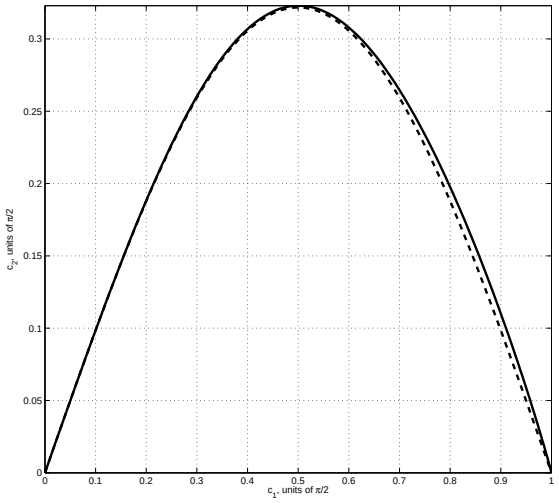

FIG. 2: Single-step steering trajectory corresponding to Fig. 1 that generates CNOT class at maximal detuning, $\delta = g$. The steering parameters are given in units of $\pi/2$. Dashed curve is for $\delta = 0$.

step implementation are given in Table II.

Figures 3 and 4 show the simulated single-step steering trajectory generated by the RWA Hamiltonian given in Eqs. (4) and (25) at $\delta = 1.5g$. Direct search for local pulses (not shown) results in the optimized gate,

$$U_{\rm opt} = \begin{pmatrix} 0.9866 & -0.1122i & 0.0258i & 0.1158 \\ -0.1122i & 0.9866 & -0.1158 & -0.0258i \\ -0.1186 & 0.0009i & 0.1122i & 0.9866 \\ -0.0009i & 0.1186 & 0.9866 & 0.1122i \end{pmatrix}, \tag{30}$$

whose intrinsic fidelity with respect to the canonical controlled-NOT gate is

$$\begin{aligned} \mathcal{F} &\equiv \sqrt{1 - {\rm tr}\left[(U_{\rm opt} - {\rm CNOT})^{\dagger}(U_{\rm opt} - {\rm CNOT})\right]} \\ &= 0.9448. \end{aligned} \tag{31}$$

TABLE I: Generation of ideal controlled-NOT logic ($G_1 = 0$, $G_2 = 1$) using capacitively coupled Josephson phase qubits at finite detuning. In the two-step case, $|\delta| \leq 2g \ll \omega$, $\Omega_1 = 0$, and $t_{(2)} = (\pi/4g)T_{(2)}$, as given in Eq. (18). In the single-step case, $|\delta| \leq g \ll \omega$. The optimal values of $\Omega_1 \approx g\sqrt{15}$ and $t_{(1)} = (\pi/2g)T_{(1)}$ have been found numerically using Nelder-Mead simplex direct search with bound constraints.

$\lvert\delta\rvert/g$	$T_{(2)}$	$T_{(1)}$	Ω_1/g
0.00	1.0000	1.0000	3.8730
0.10	1.0003	1.0009	3.8724
0.20	1.0014	1.0037	3.8707
0.30	1.0031	1.0085	3.8679
0.40	1.0056	1.0155	3.8638
0.50	1.0088	1.0253	3.8583
0.60	1.0128	1.0386	3.8513
0.70	1.0177	1.0568	3.8422
0.80	1.0235	1.0827	3.8303
0.90	1.0303	1.1245	3.8132
1.00	1.0383	1.2753	3.7781
1.10	1.0476		
1.20	1.0585		
1.30	1.0713		
1.40	1.0863		
1.50	1.1042		
1.60	1.1261		
1.70	1.1536		
1.80	1.1901		
1.90	1.2445		
2.00	1.4142		

TABLE II: Optimized values of the gate parameters for the gates closest to the single-step CNOT in the sense of Eq. (26) at $|\delta| \geq g$. Here, $t_{(1)} = (\pi/2g)T_{(1)}$. Notice how the Makhlin invariants deviate from their ideal CNOT values for larger δ.

$\lvert\delta\rvert/g$	$T_{(1)}$	Ω_1/g	G_1	G_2
1.00	1.2753	3.7781	0.0000	1.0000
1.10	1.2330	3.7470	0.0030	0.9994
1.20	1.1945	3.7323	0.0106	0.9978
1.30	1.1590	3.7250	0.0214	0.9955
1.40	1.1262	3.7203	0.0340	0.9927
1.50	1.0961	3.7152	0.0476	0.9898
1.60	1.0686	3.7074	0.0614	0.9867
1.70	1.0438	3.6952	0.0749	0.9837
1.80	1.0216	3.6772	0.0879	0.9808
1.90	1.0019	3.6519	0.1003	0.9780
2.00	0.9849	3.6179	0.1118	0.9754

VII. CONCLUSION

In summary, we have demonstrated that the CNOT pulse sequences previously proposed for resonant Joseph-

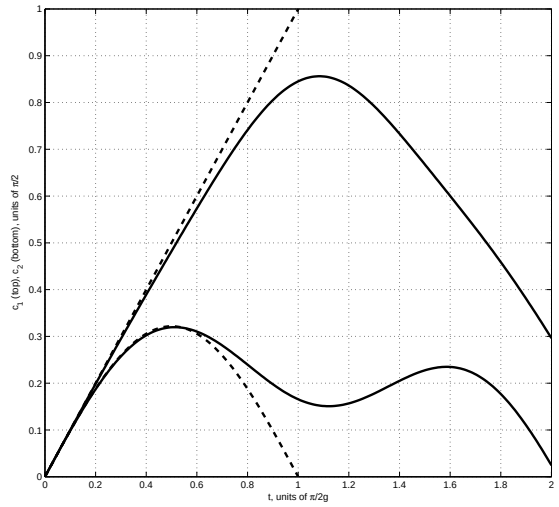

FIG. 3: Time dependence of c_1 (top curve) and c_2 (bottom curve) for single-step implementation generating the class closest to CNOT in terms of Eq. (26) at $\delta = 1.5g$. Here, $c_3 = 0$ at all times. Dashed curves represent the resonant case. Time is measured in units of $\pi/2g$. The closest class is reached at $t_{(1)} = 1.0961$.

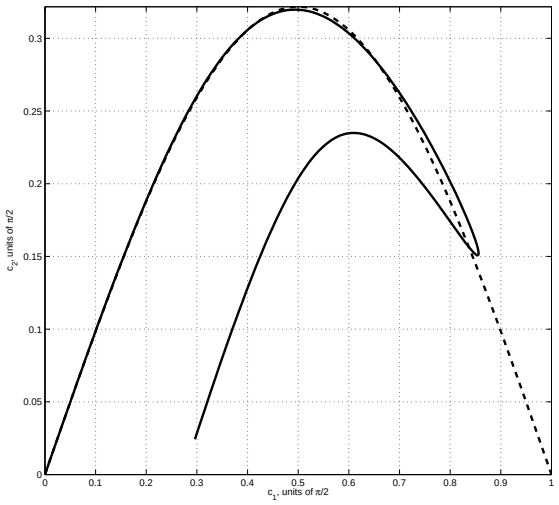

FIG. 4: Single-step steering trajectory corresponding to Fig. 3 at detuning $\delta = 1.5g$. The steering parameters are given in units of $\pi/2$. Dashed curve is for $\delta = 0$.

son phase qubits may still be used at finite detuning. To achieve high fidelity of the resulting gate the value of the detuning during the entangling operations should not be greater than $2g$ in the two-step implementation and g in the single-step implementation, respectively.

Acknowledgments

This work was supported by IARPA under grant W911NF-08-1-0336 and by the NSF under grant CMS-0404031. The author thanks Michael Geller and John Martinis for useful discussions.

[1] A. Galiautdinov, J. Math. Phys. **48**, 112105 (2007).
[2] Y. Yamamoto, Y. A. Pashkin, O. Astafiev, Y. Nakamura, and J. S. Tsai, Nature **425**, 941 (2003).
[3] A. J. Berkley, H. Xu, R. C. Ramos, M. A. Gubrud, F. W. Strauch, P. R. Johnson, J. R. Anderson, A. J. Dragt, C. J. Lobb, F. C. Wellstood, Science **300**, 1548 (2003).
[4] V. Corato, P. Silvestrini, L. Stodolsky, J. Wosiek, Phys. Rev. B **68**, 224508 (2003).
[5] J.Q.You and F. Nori, Physics Today **11**, 42 (2005).
[6] M. Steffen, M. Ansmann, R. C. Bialczak, N. Katz, E.

Lucero, R. McDermott, M. Neeley, E. M. Weig, A. N. Cleland, J. M. Martinis, Science **313**, 1423 (2006).
[7] J. H. Plantenberg, P. C. de Groot, C. J. Harmans, and J. E. Mooij, Nature **447**, 836 (2007).
[8] M. J. Testolin, C. D. Hill, C. J. Wellard, and L. C. L. Hollenberg, Phys. Rev. A **76**, 012302 (2007).
[9] A. Galiautdinov and J. M. Martinis, Phys. Rev. A **78**, 010305(R) (2008).
[10] C. Rigetti, A. Blais, and M. Devoret, Phys. Rev. Lett. **94**, 240502 (2005).
[11] J. Li, K. Chalapat, and G. S. Paraoanu, Phys. Rev. B **78**, 064503 (2008).
[12] P. R. Johnson, F. W. Strauch, A. J. Dragt, R. C. Ramos, C. J. Lobb, J. R. Anderson, and F. C. Wellstood, Phys. Rev. B **67**, 020509(R) (2003).
[13] B. L. T. Plourde, J. Zhang, K. B. Whaley, F. K. Wilhelm, T. L. Robertson, T. Hime, S. Linzen, P. A. Reichardt, C.-E. Wu, and John Clarke, Phys. Rev. B **70**, 140501(R) (2004).
[14] J. Majer, J. M. Chow, J. M. Gambetta, J. Koch, B. R. Johnson, J. A. Schreier, L. Frunzio, D. I. Schuster, A. A. Houck, A. Wallraff, A. Blais, M. H. Devoret, S. M. Girvin, and R. J. Schoelkopf, Nature **449**, 443 (2007).
[15] G. Burkard, D. Loss, D.P. DiVincenzo, and J.A. Smolin, Phys. Rev. B **60**, 11404 (1999).
[16] J. Zhang, J. Vala, S. Sastry, and K. B. Whaley, Phys. Rev. A **67**, 042313 (2003).
[17] Yu. Makhlin, Q. Inf. Proc. **1**, 243 (2003).
[18] A. Galiautdinov, Phys. Rev. A **75**, 052303 (2007).
[19] Recall that for a two-level system driven by the Hamiltonian $H = \omega_0\sigma^z/2 + g(\sigma^x\cos(\delta t) + \sigma^y\sin(\delta t))$, the corresponding time evolution operator is given by $U(t) = e^{-it\delta\sigma^z/2}e^{-it((\omega_0-\delta)\sigma^z/2+g\sigma^x)}$. Eq. (7) corresponds to $\omega_0 = 0$.